AD-A048 347 NAVAL SURFACE WEAPONS CENTER DAHLGREN LAB VA F/G 14/2
SURFACE NAVY APPLICATIONS OF MILLIMETER WAVE SENSORS. VOLUME I.--ETC(U)
NOV 77 J D HARROP, R STUMP, J J TETI

UNCLASSIFIED NSWC/DL-TR-3748 NL

1 OF 1
ADA048347

END
DATE FILMED
2-78
DDC

UNCLASSIFIED
SECURITY CLASSIFICATION OF THIS PAGE (When Data Entered)

REPORT DOCUMENTATION PAGE

READ INSTRUCTIONS BEFORE COMPLETING FORM

1. REPORT NUMBER: TR-3748 ✓
2. GOVT ACCESSION NO.:
3. RECIPIENT'S CATALOG NUMBER:

4. TITLE (and Subtitle): SURFACE NAVY APPLICATIONS OF MILLIMETER WAVE SENSORS, VOLUME I. DESIGN TRADE-OFF STUDY.
5. TYPE OF REPORT & PERIOD COVERED: Final rept.,
6. PERFORMING ORG. REPORT NUMBER:

7. AUTHOR(s): Joseph D. Harrop, Ronald Stump, John J. Teti, Jr.
8. CONTRACT OR GRANT NUMBER(s): F61112

9. PERFORMING ORGANIZATION NAME AND ADDRESS: Naval Surface Weapons Center (CF-14), Dahlgren Laboratory, Dahlgren, VA 22448 ✓
10. PROGRAM ELEMENT, PROJECT, TASK AREA & WORK UNIT NUMBERS: 62766N ZF6111200 1, CF02

11. CONTROLLING OFFICE NAME AND ADDRESS: Assistant Deputy Chief of Naval Material, Headquarters, Naval Material Command, Washington, DC 20360
12. REPORT DATE: November 1977
13. NUMBER OF PAGES: 62

14. MONITORING AGENCY NAME & ADDRESS (if different from Controlling Office): NSWC/DL-TR-3748
15. SECURITY CLASS. (of this report): Unclassified
15a. DECLASSIFICATION/DOWNGRADING SCHEDULE:

16. DISTRIBUTION STATEMENT (of this Report): 55p.

Approved for public release; distribution unlimited.

17. DISTRIBUTION STATEMENT (of the abstract entered in Block 20, if different from Report)

18. SUPPLEMENTARY NOTES

19. KEY WORDS (Continue on reverse side if necessary and identify by block number)

millimeter wave sensors
Ka band
Dicke radiometer
passive radiometer
naval applications

20. ABSTRACT (Continue on reverse side if necessary and identify by block number)

This report describes the design and construction of a test bed millimeter wave Dicke radiometer by the Naval Surface Weapons Center/Dahlgren Laboratory (NSWC/DL) during the first year of a planned two-year IED Millimeter Wave Sensor Program. The end goal of the program is to provide guidance, based on measurement data, for the selection and utilization of millimeter wave systems intended for Surface Navy applications.

(see back)

DD FORM 1 JAN 73 1473 EDITION OF 1 NOV 65 IS OBSOLETE
S/N 0102-LF-014-6601

UNCLASSIFIED
SECURITY CLASSIFICATION OF THIS PAGE (When Data Entered)

391 598

1B

(20)

This report includes discussions of program background, related Department of Defense (DOD) programs, system limitations, and projected test plans for FY 78. Volume II, NSWC/DL TR-3749 (classified CONFIDENTIAL), contains detection range predictions.

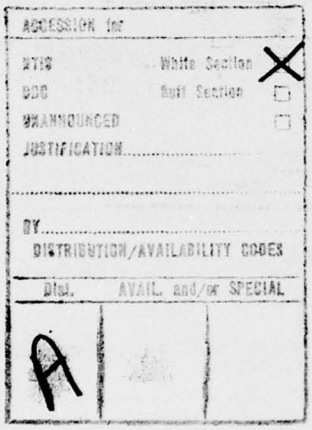

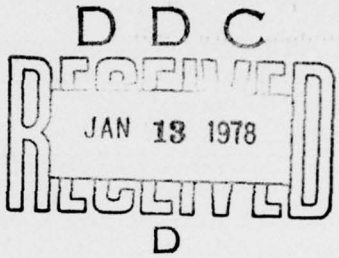

FOREWORD

Increased military interest in millimeter wave technology has produced the requirement for more complete propagation data and improved millimeter wave component performance in order to better develop and utilize millimeter wave systems.

This report covers the work performed by NSWC/DL during the first year of a two-year IED program to study the utility of millimeter wave systems for the Surface Navy. Volume II, NSWC/DL TR-3749, contains the confidential detection range predictions for the radiometer that was constructed.

This report was reviewed for technical accuracy by the following personnel of the Advanced Projects Division, Electronics Systems Department:

R. W. Dorsey, Head, Surface Weapons Technology Branch
O. F. Braxton, Head, Advanced Projects Division

Released by:

R. T. RYLAND, JR., Acting Head
Electronics Systems Department

TABLE OF CONTENTS

INTRODUCTION

Many millimeter wave systems have been built in the past to perform various tasks. These systems have been successful and significant, especially in the field of radio astronomy. The basic utility of millimeter wave systems as applied to the Surface Navy, however, is currently undefined. The overall goal of the IED Millimeter Wave Sensor Program is to determine the basic utility that millimeter wave systems might have for the Navy in general and, in particular, the applications that passive millimeter wave sensors might have for the Surface Navy. The basic approach is to establish in-house millimeter wave expertise with an accompanying test program to expand the data base established by related NSWC/DL programs. These test results can then be used to specify future millimeter wave development efforts. This portion of a two-year program is devoted to the construction of a test bed passive system intended for use in the measurements and analysis portion of the program to be completed in FY 78.

The test bed system will consist of a 35-GHz passive radiometer mounted on a fully instrumented, precision tracking mount. Presently, this system is intended for a variety of study applications to improve the Navy's expertise and data base for military applications of millimeter wavelength systems. Areas of interest at this time are:

1. Measurements of sky temperature profiles
2. Measurements of sea temperature profiles
3. Measurements of interface profiles between sky, sea, and land masses
4. Signature measurements of calibration targets, simple reference targets, ship targets, and air targets
5. Slow scan imagery of calibration targets and ship targets
6. Detection range measurements of ship and air targets
7. Harbor surveillance and navigation
8. Passive communications

All these data will be taken to include the effects of aspect angle, sea state, weather/cloud cover, and polarization. These study areas and their parameters will have a pronounced effect on the system design to follow.

PROGRAM OVERVIEW

BACKGROUND AND RATIONALE

Historically, the Navy has relied on both optical and radar systems to detect, identify, and designate airborne and surface targets. Radar systems have been limited to X-band frequencies and below because of device availability, performance, and system requirements. However, the improved performance of ship defense penetrators and weapon systems makes it necessary to increase the ability of ships to classify and respond to these threats. A number of options are available to the system designer, each with its own characteristic limitations. The basic limitations, however, are those associated with resolution, antenna gain, antenna side-lobe level, and multipath and clutter phenomena.

Multipath and clutter in the at-sea environment are due, primarily, to the fact that antenna main beam and side-lobe patterns cannot be ideally shaped. Much of a radar's power is transmitted and received in these side-lobes, resulting in ambiguous returns from the sea surface (clutter) and long path reflections of the target return from the sea surface (multipath).

Angular resolution is also a function of aperture size. For a given frequency, assuming the signal processing is optimized, the theoretical resolution can be increased only by increasing the antenna aperture.

These problems can be resolved at lower frequencies, at the expense of shipboard real estate, by increasing the size of the radar antenna. Optical and electro-optical systems can be and are used to overcome these problems in some cases, although they can be severely limited by weather. Another possible solution is the use of some stand-alone system or combination of microwave, millimeter wave, and optical (or electro-optical) systems.

Millimeter wave systems could provide a variety of advantages such as small antenna size with very narrow beam widths, nearly all-weather capability, active or

passive mode of operation, small rugged components, and the possibility of non-real time imaging. These qualities make possible a number of applications including:

1. High resolution tracking fire control radar

2. Slow scan target identification imagery

3. Very low elevation tracking over water

4. Covert operation, immune to standoff jammers (operation near an atmospheric absorption frequency)

5. Small active or passive seekers for guided weapons

The ability to establish the desirability and feasibility of the above and similar applications is one of the ultimate capabilities that should result from this program effort combined with other related programs at NSWC/DL. These and DOD related programs are the subject of the next two sections.

DOD EFFORTS IN MILLIMETER WAVE TECHNOLOGY

All three DOD services, Army, Air Force, and Navy, have ongoing programs exploiting millimeter wave technology. The Army and Air Force are primarily concerned with using millimeter wave seekers against a massed armor attack in Europe, while the Navy is interested in millimeter wave radar for fire control applications and millimeter wave communications. Various agencies and their known millimeter wave efforts are discussed below. A detailed analysis of the various programs is beyond the intended scope of this report, so only the basic lines of research will be identified without further comment.

Air Force

The Space and Missile Systems Organization (SAMSO) has several programs using millimeter waves for detection of reentry vehicles and identification and imaging of satellites. Another major Air Force agency employing tactical millimeter wave applications is the Air Force Armament Technology Laboratory (AFATL), Eglin Air Force Base, Florida. Of AFATL's several millimeter wave guidance programs, the primary program is the Millimeter Contrast Guidance (MCG) Program, with Honeywell and others as prime contractors for the various program elements.

Other AFATL programs include: MTT (Moving Target Tracker), which uses millimeter waves as a moving target discriminator, and WAM (Wide Area Munition), which uses millimeter wave systems against massed armor. AFATL is also investigating various phenomenology at millimeter wavelengths, primarily atmospheric propagation, land and snow clutter.

The Air Force Avionics Laboratory (AFAL) at Wright-Patterson Air Force Base, Dayton, Ohio, has several programs in millimeter wave solid-state and tube technology. AFAL is pushing for higher powers, wider bandwidths, and better noise properties in all their component efforts.

Army

The Army has several ongoing millimeter wave programs, primarily at the Army Missile Command (MICOM), Huntsville, Alabama; the Harry Diamond Laboratories (HDL), Adelphi, Maryland; the Night Vision Laboratory (NVL), Fort Belvoir, Virginia; and Picatinny Arsenal, Dover, New Jersey. The Army has a ballistic missile defense program at the Ballistic Missile Defense Advanced Technology Center (BMDATC) and several tactical programs at other locations. SADARM, for example, a program at Picatinny Arsenal, is an antitank millimeter wave passive sensor deployed against massed armor. Both 35- and 94-GHz seeker development is ongoing at MICOM. MICOM is also taking clutter data and target signature data at 35 and 94 GHz. A considerable amount of submillimeter and millimeter work is ongoing at HDL including funding of some of the Gyro Traveling-Wave Tube (TWT) development work at the Naval Research Laboratory (NRL), Washington, D. C. (see the next section). A millimeter wave fire control radar for tanks, project STARTLE, is under development at NVL. The Ballistic Research Laboratories (BRL), Aberdeen, Maryland has under development a 140- and a 217-GHz beamrider missile for antitank applications.

Navy

Navy millimeter wave efforts are mainly oriented toward improving communication, component, and radar technology. The Naval Ocean Systems Center (NOSC), San Diego, California has several ongoing programs in millimeter wave components pushing development of improved Gunn and Impatt diodes and low loss transmission lines. NOSC also has a program for millimeter wave ship-to-ship, ship-to-land, etc., communication. The Naval Air Development Center (NADC), Warminister, Pennsylvania, has developed a 95-GHz instrumentation radar which has

been used in several tests, particularly rain backscatter tests. NRL has had several programs in millimeter wave technology; a current NRL program is developing a dual X-band, Ka-band common aperture range instrumentation radar. NRL is pushing state of the art in solid-state and tube components at the millimeter frequencies. A Gyro TWT, a very high power millimeter wave tube, and some millimeter TWT's for electronic countermeasures (ECM) applications are being developed by NRL. NRL is also working with solid-state millimeter wave component technology development. The Naval Weapons Center (NWC), China Lake, California is developing passive millimeter wave navigation techniques using stored optical reference maps to correlate with real-time millimeter wave images of an area for the purpose of determining the relative location of an airborne platform. NWC is also developing a four-channel, strip-line microwave integrated circuit receiver for guidance and mapping applications. NSWC is also engaged in developing millimeter wave technology; these programs are discussed in more detail later.

Defense Advanced Research Projects Agency (DARPA)

The Defense Advanced Research Projects Agency (DARPA), Arlington, Virginia, is heavily involved with millimeter wave development. DARPA is funding development of millimeter wave technology in three areas: (1) components for tactical applications; (2) seekers; and (3) strategic applications for ballistic missile defense. A major DARPA program has been the Semiactive Guidance Program, with Sperry and Norden as contractors. In this program, a cannon-launched guided projectile homes on a target which has been illuminated by a remotely piloted vehicle (RPV). DARPA's Strategic Technology Office also has several millimeter wave programs for space object identification and ballistic missile defense.

Coast Guard

Another agency using millimeter wave technology, although not for military applications, is the U. S. Coast Guard. The Coast Guard has a Ka-band passive radiometer on board a flying boat for oil slick detection and surveillance. The Coast Guard also has a 95-GHz radar used for harbor surveillance.

DIRECTLY RELATED NSWC PROGRAMS

Microwave Radiometric Terminally Aimed Bomb (MICRAD TAB) Study

The MICRAD TAB program at NSWC/DL evaluates millimeter wave guidance concepts for low-cost, all-weather, strap-on guidance kits compatible with laser-guided bomb (LGB) airframes. Because laser-guided weapons are weather-limited,[1] a seeker

utilizing a longer wavelength becomes an attractive choice as an alternative seeker to be used during these adverse weather conditions. However, very high resolution for target discrimination is required. Therefore, millimeter wavelength seekers seem desirable. Another attractive feature of the millimeter wavelength spectrum is that it enables the use of passive radiometric target discrimination.

The new LGB PEP airframe has been chosen as the vehicle for analysis because of its high maneuverability. A "first-cut" analysis has determined the maneuver limitations of the vehicle itself, the required seeker field of view set to cover the maneuver footprint, and the required seeker acquisition range to maneuver to a specified percentage of targets. Analysis of the millimeter wave seeker has been done to determine passive radiometric, semiactive, and active performance. A preliminary cost analysis has also been completed. Seeker limitations, weather effects, and hardware state of the art were all examined to determine their effects upon a millimeter wave system. Recommendations and conclusions of the effort will be presented in a forthcoming NSWC/DL technical report.[2]

Millimeter Wave Block Program Work Unit

The millimeter wave block program work unit was initiated at the beginning of FY 77 to determine feasibility of using millimeter wavelength radar for point defense capability against low elevation targets. This broad objective has been addressed in two areas: (1) establishment of a data base which is solid in theory and applicable to the problems of the Surface Navy and (2) identification of hardware development efforts which will advance component technology, where feasible, to a level where millimeter wavelengths can best be used to solve Surface Navy requirements, particularly the low-altitude threat. As part of the block program millimeter wave effort, the following projects are funded or planned for funding at this time.

1. Propagation Data Base Formulation, performed by the Illinois Institute of Technology Research Institute, describes the atmospheric interaction upon the beam to enable both a level of performance prediction and a model which will aid in the design of the tracking and threshold loops within a radar system. This effort has been successfully concluded.

2. Sea Clutter Modeling, being conducted by the Georgia Institute of Technology, will also aid in both the prediction of performance and the design of tracking loops in that it will statistically describe the characteristics of the interaction of the radio frequency (RF) beam and the sea surface for a wide range of environmental conditions.

3. The above two efforts, when combined with the NSWC/DL in-house data base formulation, will form the basis for planned system trade-off studies of proposed millimeter wave concepts during FY 78. As part of this effort, the models and simulations generated under contracts will be incorporated into an overall system model to be placed on the CDC 6700 computer at NSWC/DL.

4. To achieve advancement in hardware state of the art, the area identified as critical to any future concept for millimeter wave shipborne systems is generation of high peak and average power levels from a reliable source. Current devices, such as a magnetron, are limited to about 100-kW peak, 100-W average power at 40 GHz and 10-kW peak, 2-W average power at 95 GHz. The current technology magnetron at 94 GHz has a lifetime, at best, of only a few hundred hours. As with magnetrons at lower frequencies, the devices are not coherent on a pulse-to-pulse basis; thus, a system for MTI is made difficult. Two new devices, an Extended Interaction Amplifier (EIA) and a Gyro TWT, show promise as possible solutions to these problems by providing significant power gains at millimeter wavelengths. Development of both of these new devices is being supported within the block effort. An application study by NRL for their Gyro TWT is being funded by the NSWC/DL effort, while the tube development cost is being funded by the Naval Electronics Systems Command (NAVELEX). NSWC/DL is now assessing the technology of the EIA for possible development. The Gyro TWT, being investigated by the Plasma Physics Division at NRL, should be capable of very high peak and average powers. NRL is currently building the first prototype to operate at 35 GHz, and it should be capable of 200-kW peak and 10-kW average power in a production model. Since the Gyro TWT is also a coherent amplifier, doppler processing can be employed for the MTI function. The EIA also offers promise to the millimeter wave design engineer. This device, a modification of the Klystron design, is being developed by Varian Canada and will reportedly be capable of 30-kW peak, 1-kW average power at 35 GHz. This is an order of magnitude greater than that achievable with current magnetron devices, yet, the EIA promises to outlive current magnetrons by a factor of 10 to 100. With the increased average power of the EIA, pulse compression techniques can be used to increase the effective peak power above that of current magnetron devices, without the problems of waveguide breakdown associated with actual high peak power systems.

A major importance of the in-house IED program is its relation to the block effort, the final goal of which is to field a fire control system for the Surface Navy. This is not a single-step operation, however; it requires several smaller learning steps. The IED effort fulfills the first of these steps in that it establishes a baseline system and provides a test bed for further hardware improvements expected from programs such as the block effort.

NSWC/WO IED Effort

A program closely related to Dahlgren's effort is one by the NSWC/White Oak Laboratory (NSWC/WO) which is involved with building an active 35-GHz monopulse radar tracking system to be completed and tested in FY 78. Coordination is being made between these two programs to best utilize the two sets of talents involved and to expand the resulting data base. As a result of White Oak's effort, the active element of the original Dahlgren effort has been halted in favor of using NSWC/WO results. These results, which will be made available later, should adequately demonstrate the capabilities of active millimeter wave tracking systems as well as point out areas of needed improvements in technology and methodology.

APPROACH

THE RADIOMETRIC EFFECT

All objects above absolute zero, or 0°K, radiate, absorb, and reflect energy. A blackbody is a body which is a perfect emitter and absorber of energy. The brightness of blackbody radiation is given by Planck's radiation law which states that the brightness of a blackbody radiator at temperature T and frequency f is given by:

$$B = \frac{2hf^3}{c^2} \frac{1}{e^{(hf/kT)} - 1} \qquad (1)$$

where

h = Planck's constant, 6.63×10^{-34} J/sec
k = Boltzman's constant, 1.38×10^{-23} J/K°
c = velocity of light, 3×10^{8} m/sec
f = frequency, Hz
B = brightness, watts m^{-2} Hz^{-1} rad^{-2}
T = temperature, °K

In the millimeter wave region of the electromagnetic spectrum the Rayleigh-Jeans approximation is applicable, $hf \ll kT$, and Equation 1 reduces to:

$$B = \frac{2hf^3}{c^2} * \frac{kT}{hf} = \frac{2\,kT}{\lambda^2} \tag{2}$$

where

λ = wavelength

Thus, brightness is proportional to $1/\lambda^2$ and to the temperature of the object. Blackbody, Planck-law radiation curves are shown in Figure 1 for temperatures of 6000 and 12,000°K, and Figure 2 shows a group of curves plotted logarithmically by Kraus.[3] The brightness curves are approximately linear in temperature in the region greater than 1 mm in wavelength. The radiometric temperature of a blackbody, perfect emitter, is equivalent to its absolute thermodynamic temperature. In contrast, a perfect reflector emits no radiation characteristic of its thermodynamic temperature. Thus, a measure of radiation from a perfect reflector is a measure of the radiation from the surroundings by reflection. Most objects are neither perfect reflectors nor perfect emitters; their radiometric temperature is a function of their actual thermodynamic temperature and the temperature of the reflected surroundings. These bodies, called gray bodies, have a radiometric temperature given by:

$$Tg = (1 - \rho)T_{obj} + \rho T_B \tag{3}$$

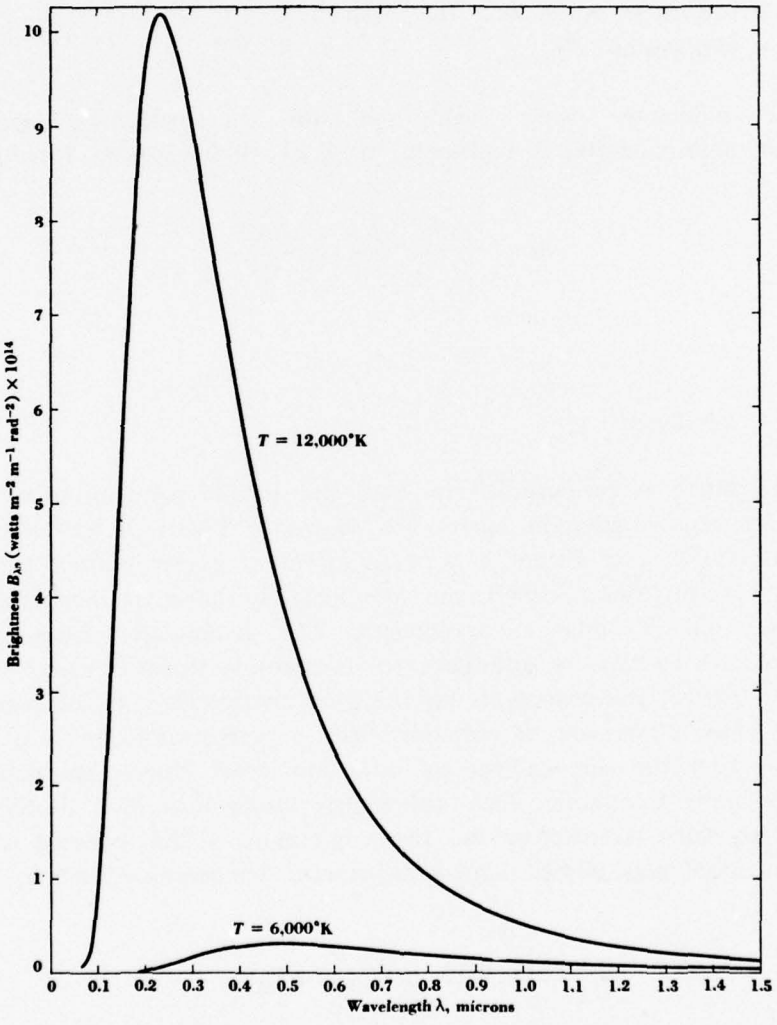

Figure 1. Planck-Radiation-Law Curves at 6000 and 12,000°K[3]

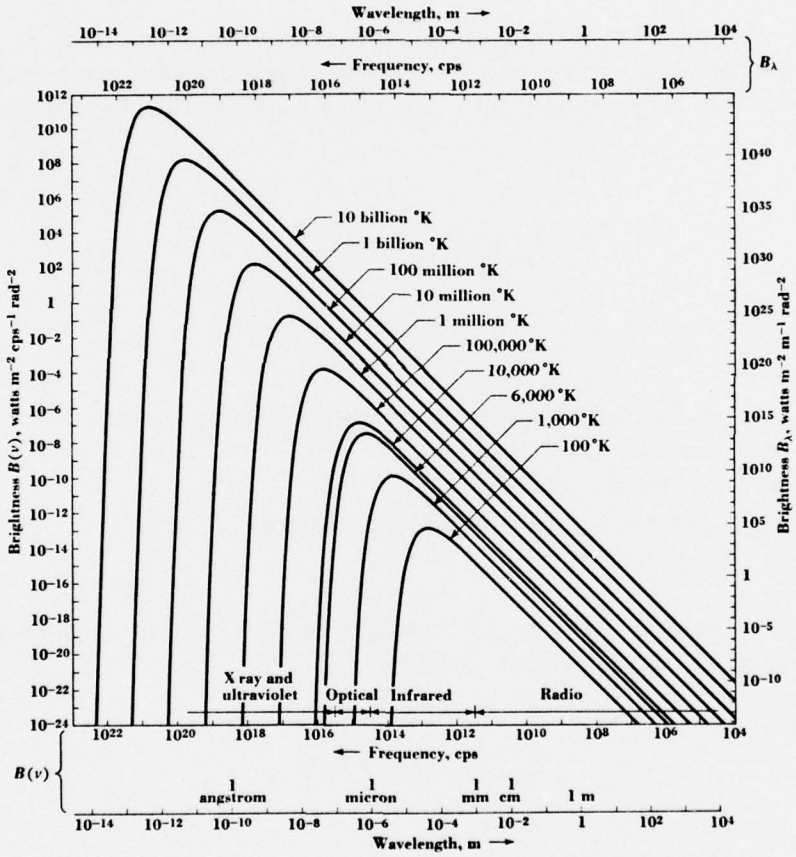

Figure 2. Planck-Law Radiation Curves to Logarithmic Scales With Brightness Expressed as a Function of Frequency B (ν) (Left and Bottom Scales) and as a Function of Wavelength Bλ (Right and Top Scales). Wavelength Increases to the Right[3]

where

T_g = radiometric temperature of the object
T_{obj} = thermodynamic temperature of the object
T_B = thermodynamic temperature of the background
ρ = reflection coefficient

The quantity $1 - \rho$ is called emissivity, ϵ.

If, for now, path losses are neglected, the receiving antenna beam is assumed to just cover a target with reflectivity, ρ, and the target is viewed such that it reflects predominately sky temperatures, then the temperature sensed by the radiometer is given by:[4]

$$T_{eqT} = \epsilon_T T_T + \rho_T T_{sky} \tag{4}$$

where

T_{eqT} = radiometric temperature of target seen by antenna
ϵ_T = emissivity of target
ρ_T = reflectivity of target
T_T = thermodynamic temperature of target
T_{sky} = sky temperature

The radiometric temperature of the background seen by the radiometer as the antenna looks at the background is given by:

$$T_{eqB} = \epsilon_B T_B + \rho_B T_{sky} \tag{5}$$

where

T_{eqB} = radiometric temperature of background seen by antenna
ϵ_B = emissivity of background
ρ_B = reflectivity of background
T_B = thermodynamic temperature of background

The radiometric target contrast is the temperature differential between the observed target temperature and the observed background temperature.

$$\Delta T = T_{eqB} - T_{eqT} \tag{6}$$

$$= \epsilon_B T_B + \rho_B T_{sky} - \epsilon_T T_T - \rho_T T_{sky} \tag{7}$$

$$= \epsilon_B T_B - \epsilon_T T_T + T_{sky}(\rho_B - \rho_T) \tag{8}$$

From Equation 8, the temperature contrast between two bodies is a function of their physical temperatures, emissivities, reflectivities, and the sky temperature. If two bodies are of identical physical temperature, a temperature contrast can still exist provided their reflectivities are different. In the millimeter wavelength portion of the electromagnetic spectrum $\rho \simeq 1$ and $\epsilon \simeq 0$ for metals, while ρ tends to be small and ϵ approaches 1 for natural backgrounds. The apparent temperature of metal objects can therefore be low when its radiometric temperature is determined primarily by sky temperature reflections. A natural background will have a high apparent temperature since its emissivity is high and reflectivity is low. This apparent temperature contrast is used as the target discriminant for passive systems.

LIMITING FACTORS

Beam Fill Effects

Most realistic target conditions encountered are limited by target beam fill effects and path loss due to weather conditions. A non-beam filling condition, the angle subtended at the antenna by the target being less than the antenna beam width, has the effect of reducing the target to background contrast by increasing the amount of unwanted background energy received while observing the target. From Reference 4, the effective antenna temperature is:

$$T_{antT} = \frac{\Omega_T}{\Omega_B} T'_{eqT} + \frac{\Omega_B - \Omega_T}{\Omega_B} T'_{eqB} \tag{9}$$

where

T_{antT} = effective antenna temperature
T'_{eqT} = loss-corrected target radiometric temperature
T'_{eqB} = loss-corrected background radiometric temperature
Ω_T = solid angle subtended at the antenna by the target
Ω_B = solid angle subtended by the antenna beam

It becomes apparent that for $\Omega_T < \Omega_B$, the effective antenna temperature is dependent on both the target and background temperatures and, in fact, is increased by any non-zero background temperature. This weighting of antenna temperature, in effect, reduces target-to-background contrast.

Before considering path loss effects, the effects of weather on atmospheric attenuation and the relative extent of these weather effects will be discussed.

Weather

Before a millimeter wave system can be designed, the effects of weather upon propagation must be known and accounted for. The primed terms of Equation 9 are radiometric temperatures that have been corrected for path loss. These path losses are primarily a function of water vapor and oxygen content in the atmosphere. Rain, haze, fog, and atmospheric temperature are also significant factors affecting propagation at these frequencies.

In the millimeter spectrum, the operating wavelength tends to be of the same order of magnitude as the diameter of the particulate water droplets. Table 1 shows drop diameters for various atmospheric conditions. This resonant region operation can cause significant atmospheric attenuation and signal backscatter.[6] Weather effects can be reduced to some extent in active systems through the use of circularly polarized, high gain, narrow beam width antennas and short transmitter pulse widths. Rain, fog, and water vapor will be considered for their effects on propagation at millimeter frequencies.

Table 1. Drop Diameters for Various Atmospheric Conditions[5]

Atmospheric Condition	Drop Size Range (μm)
Haze	0.01 – 3
Fog	0.01 – 100
Clouds	1 – 50
Drizzle (0.25 mm/hr)	3 – 800
Moderate Rain (4.0 mm/hr)	3 – 1500
Heavy Rain (16.0 mm/hr)	3 – 3000

Rosenblum[7] has shown attenuation rates versus frequency from 10 to 400 GHz for propagation at sea level and 4 km altitude. Attenuation versus pressure, temperature, and water vapor content are shown in Figure 3. The regions of increased attenuation are at 22, 60, 120, and 183 GHz. These regions occur where the energy propagated excites molecular motion in oxygen or water vapor molecules. The peaks shown in Figure 3 correspond to discrete lines of attenuation at specific frequencies, but are broadened by the effects of atmospheric pressure and its changes.

Tables 2 and 3 list discrete values of frequency for the various molecular transition states excited in the oxygen or water vapor molecules. Figure 3 is valid for clear air and the parameters shown but does not consider increased attenuation due to rain.

Much research has been conducted to study the effects of rain upon millimeter wave propagation.[5] In most cases, the measured data taken by the various researchers to date appear to be in general agreement with predicted data. Georgia Institute of Technology has calculated data on rain attenuation at 10, 35, 70, and 95 GHz;[9] their results are shown in Figure 4. For one-way path loss, the figure of 1 dB/km attenuation at rain rates of 4 mm/hr appears to be representative of rain attenuation in moderate rain at 35 GHz. As expected, signal attenuation depends upon rain rate, rain cell size, droplet size, droplet distribution, and increased humidity during a rain storm.[10]

UPPER CURVE

SEA LEVEL

P = 760mm Hg

T = 20°C

pH_2O = 7.5 g/m^3

LOWER CURVE

4 KM ABOVE SEA LEVEL

T = 0°C

pH_2O = 1.0 g/m^3

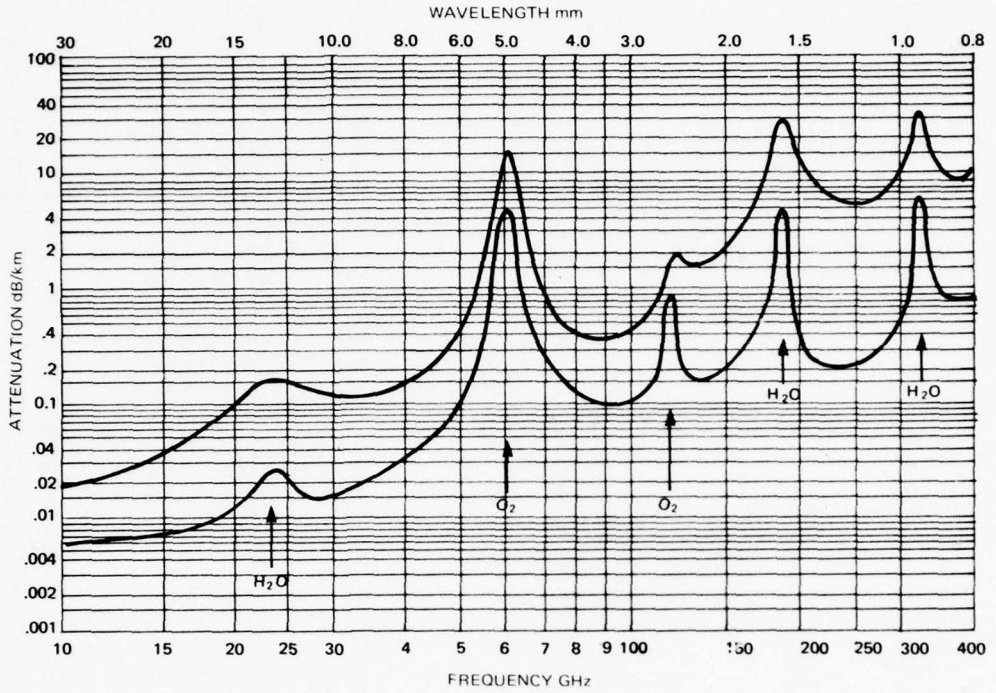

Figure 3. Average Atmospheric Absorption of Millimeter Waves (Horizontal (Propagation)[8]

Table 2. Transition Frequencies for Oxygen Absorption[8]

N	ν_{N+} (MHz)	ν_{N-} (MHz)
1	56,264.7	118,750.7
3	58,446.9	62,486.7
5	59,591.5	60,306.1
7	60,435.5	59,164.0
9	61,151.3	58,323.6
11	61,800.9	57,612.1
13	62,411.9	56,967.8
15	62,998.5	56,363.1
17	63,568.7	55,783.6
19	64,127.6	55,221.5
21	64,678.2	54,671.6
23	65,222.7	54,130.9
25	65,762.6	53,597.3

Table 3. Water Vapor Absorption Frequencies and Associated Data[8]

Frequency (GHz)	ϵ_{op}	γ_{op} (dB/km)
22.2	0.110	0.14
183.6	0.510	27.6
325.8	0.210	31.5
380.1	0.350	297
449.4	0.244	308
557.4	0.889	19,600
753.3	0.708	13,200
987.9	0.833	9,710
1097.7	0.509	63,500
1113.9	1.0	19,650
1164.0	0.424	69,400

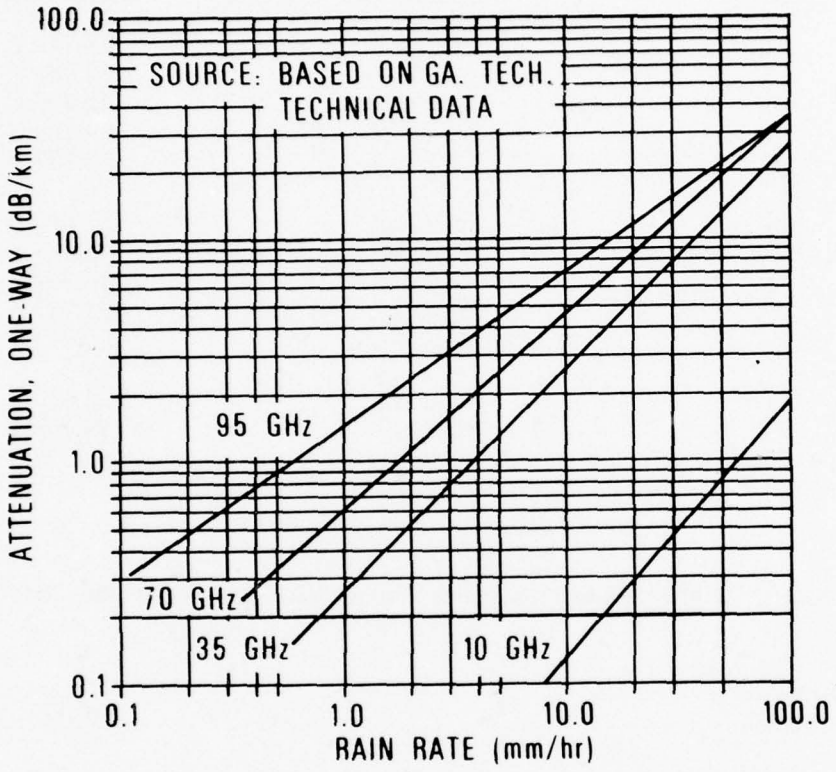

Figure 4. Atmospheric Attenuation Versus Rain Rate[9]

Attenuation of millimeter waves by fog has been addressed by Koester and Kosowsky.[11] Table 4 shows the characteristics of both inland and coastal fog. The parameters listed are all typical, general numbers. Only on rare occasions does the liquid water content approach 0.5 to 1 gm/m^3, and this occurs in very dense radiation fogs with 20- to 30-m visibility. An equation[11] has been derived to calculate the attenuation coefficient for propagation in fog and is given by:

$$\alpha = \frac{81.86\ M\ \mathrm{Im}(-K)}{\lambda \rho}\ \mathrm{dB/km} \qquad (10)$$

$$K = \frac{m^2 - 1}{m^2 + 1} \qquad (11)$$

where

m = complex index of refraction
M = liquid water content per unit volume of fog in g/m^3
λ = wavelength in mm
ρ = density of water in gm/cm^3

Table 4. Fog Characteristics[11]

Description	Radiation (Inland) Fog	Advection (Coastal) Fog
Average Drop Diameter (μm)	10	20
Typical Drop Size Range (μm)	5-35	7-65
Liquid Water Content (g/m^3)	0.11	0.17
Droplet Concentration (per cm^3)	200	40
Visibility (m)	100	200

Raleigh scattering criteria are satisfied with this equation because the droplet size is much smaller than the wavelength; therefore, the equation can be used. The water density used in the equation is generally 1 gm/m^3. A listing of complex index of refraction is shown in Table 5. From Equation 10, absorption coefficients for water are calculated and are listed in Table 6. Figure 5 shows the attenuation values (listed in Reference 5) for fog as a function of liquid water content and illustrates that only under rare conditions can the attenuation coefficient of fog approach the value used (1 dB/km) for propagation in 4 mm/hr of rain. A more typical value would be either 0.11 dB/km for inland radiation fog or 0.17 dB/km for an advection coastland fog. As a means of comparison, Figure 6 plots visibility versus liquid water content for radiation and advection fogs. Thus, for "typical" values of liquid water content, 0.11 and 0.17 gm/m^3, visibilities of 100 and 200 m, respectively, are shown.

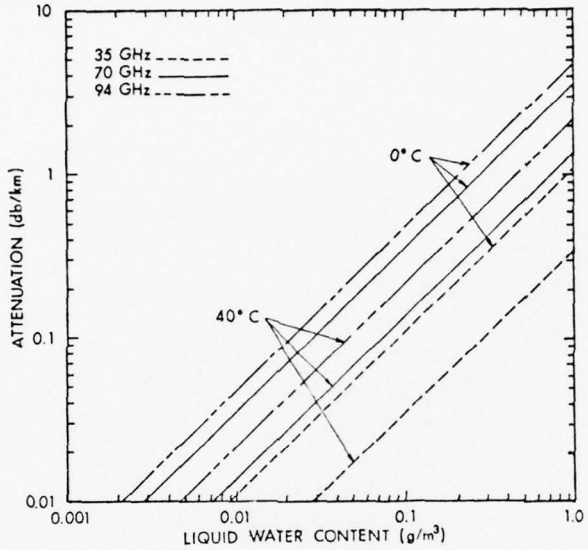

Figure 5. One-Way Attenuation in Fog as a Function of Liquid Water Content[5]

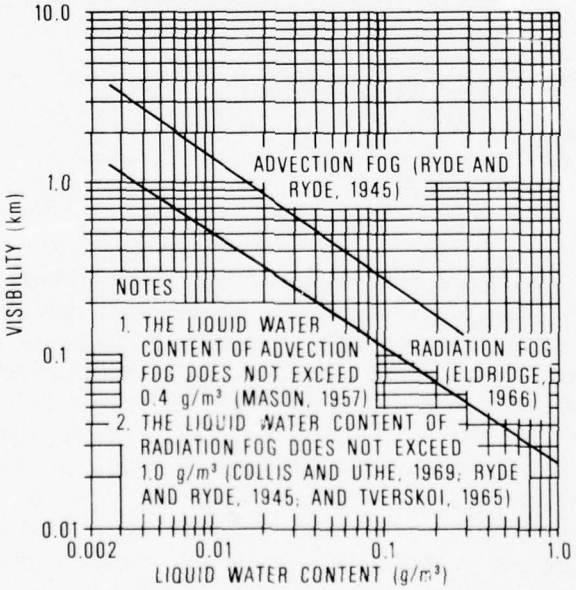

Figure 6. Correlation of Visibility in Fog to Liquid Water Content[11]

Table 5. Complex Index of Refraction of Water[5]

Temperature (0°C)	8.6 mm 35 GHz	4.3 mm 70 GHz	3.2 mm 94 GHz
0	3.947 – j2.367	3.039 – j1.603	2.801 – j1.302
10	4.802 – j2.735	3.543 – j2.059	3.173 – j1.732
20	5.607 – j2.838	4.077 – j2.380	3.596 – j2.076
30	6.266 – j2.733	4.608 – j2.574	4.031 – j2.323
40	6.748 – j2.501	5.108 – j2.649	4.457 – j2.477

Table 6. Absorption Coefficients for Water[5]

Temperature (0°C)	Absorption Coefficient 35 GHz	70 GHz	94 GHz
0	0.114	0.172	0.183
10	0.079	0.137	0.162
20	0.058	0.107	0.133
30	0.044	0.085	0.109
40	0.036	0.069	0.090

Backscatter is another effect that occurs due to atmospheric particulates. However, since backscatter has a minor effect on passive systems, it will not be discussed in this report. A detailed backscatter analysis is given in Reference 2.

Path Loss Effects

As the radiometric temperature of a gray body is observed through a medium, such as the atmosphere, the radiometric energy transmitted by the body is attenuated. The medium itself also has a radiometric temperature which would change the apparent temperature of the gray body as seen by a radiometer. From the preceding discussion of weather effects, it is evident that path losses can be significant at millimeter wavelengths. These losses affect the detected radiometric temperature as:[4]

$$T_{out} = \frac{T_{in}}{L} + T_{amb}\frac{(L-1)}{L} \tag{12}$$

where

T_{out} = received radiometric temperature
T_{in} = target radiometric temperature
L = loss factor of medium
T_{amb} = thermodynamic temperature of the medium

Substituting the proper terms into Equation 12 yields the loss-corrected terms, T'_{eqT} and T'_{eqB}, as:

$$T'_{eqT} = \frac{T_{eqT}}{L} + T_{amb}\frac{(L-1)}{L} \tag{13}$$

and

$$T'_{eqB} = \frac{T_{eqB}}{L} + T_{amb}\frac{(L-1)}{L} \tag{14}$$

where

T_{eqT} = radiometric target temperature
T_{eqB} = radiometric background temperature

Now, substituting Equations 13 and 14 into Equation 9 yields:

$$T_{antT} = \frac{\Omega_T}{\Omega_B}\left[\frac{T_{eqT}}{L} + T_{amb}\frac{(L-1)}{L}\right] + \left(\frac{\Omega_B - \Omega_T}{\Omega_B}\right)\left[\frac{T_{eqB}}{L} + T_{amb}\frac{(L-1)}{L}\right] \quad (15)$$

where

T_{antT} = effective antenna temperature
T_{eqT} = radiometric target temperature
T_{eqB} = radiometric background temperature
T_{amb} = thermodynamic temperature of medium
Ω_T = solid angle subtended at the antenna by the target
Ω_B = solid angle subtended by the antenna beam

A complete expression for target contrast can now be developed. The difference between the observed target temperature and the observed background temperature is defined as the resolvable target contrast. Not considering beam fill and path losses, this can be expressed as:

$$\Delta T_{eqT} = |T_{eqT} - T_{eqB}| \quad (16)$$

where

ΔT_{eq} = target contrast
T_{eqT} = uncorrected target radiometric temperature
T_{eqB} = uncorrected background radiometric temperature

Substituting the loss-corrected terms into Equation 16 and allowing for non-beam filling results in:

$$\Delta T_{eqT} = \left| T_{antT} - \left(\frac{\Omega_B}{\Omega_B}\right)\left[\frac{T_{eqB}}{L} + T_{amb}\frac{(L-1)}{L}\right]\right| \quad (17)$$

where T_{antT} becomes the loss-corrected term for T_{eqT}, and T_{eqB} becomes the right half of Equation 14 corrected for beam fill, in which Ω_B/Ω_B becomes 1 for the background. This can next be expanded to produce:

$$\Delta T_{eqT} = \left| \left(\frac{\Omega_T}{\Omega_B}\right)\left[\frac{T_{eqT}}{L} + T_{amb}\frac{(L-1)}{L}\right] + \left(\frac{\Omega_B - \Omega_T}{\Omega_B}\right)\left[\frac{T_{eqB}}{L} + T_{amb}\frac{(L-1)}{L}\right] - \left(\frac{\Omega_B}{\Omega_B}\right)\left[\frac{T_{eqB}}{L} + T_{amb}\frac{(L-1)}{L}\right] \right| \quad (18)$$

which reduces to

$$\Delta T_{eqT} = \left| \left(\frac{\Omega_T}{\Omega_B}\right)\left[\frac{T_{eqT}}{L} + T_{amb}\frac{(L-1)}{L}\right] - \left(\frac{\Omega_T}{\Omega_B}\right)\left[\frac{T_{eqB}}{L} + T_{amb}\frac{(L-1)}{L}\right] \right| \quad (19)$$

and further reduces to

$$\Delta T_{eqT} = \left| \left(\frac{\Omega_T}{\Omega_B}\right)\frac{(T_{eqT} - T_{eqB})}{L} \right| \quad (20)$$

Earlier, Equation 8 stated that contrast, neglecting beam fill effects and path loss, is given by:

$$\Delta T = \epsilon_B T_B - \epsilon_T T_T + T_{sky}(\rho_B - \rho_T) \quad (21)$$

where

ϵ_B = emissivity of background
ϵ_T = emissivity of target
$\rho_B = 1 - \epsilon_B$ = background reflectivity
$\rho_T = 1 - \epsilon_T$ = target reflectivity
T_B = thermodynamic temperature of background
T_T = thermodynamic temperature of target
T_{sky} = radiometric sky temperature

Equation 20 can similarly be rewritten in terms of background and target reflectivities and emissivities as:

$$\Delta T = \left| \left(\frac{\Omega_T}{\Omega_B} \right) \left[\frac{(\epsilon_T T_{eqT} + \rho_T T_{sky}) - (\epsilon_B T_{eqB} + \rho_B T_{sky})}{L} \right] \right| \tag{22}$$

And if, as stated earlier, for metal targets $\rho_B \simeq 0$ and $\epsilon_T \simeq 0$, then this equation reduces to:

$$\Delta T_{eqT} \simeq \left| \left(\frac{\Omega_T}{\Omega_B} \right) \frac{(\rho_T T_{sky} - \epsilon_B T_{eqB})}{L} \right| \tag{23}$$

This equation, or Equation 14, is now in a form which is useful for predicting the contrast that can be expected for any particular radiometric system. This allows a reasonable prediction of theoretical detection capabilities to be made prior to the system design.

As shown, total power seen by a radiometer can thus be affected by the following factors:

1. Target temperature
2. Background temperature
3. Sky temperature
4. Path considerations
5. Target emissivity
6. Background emissivity
7. Antenna beam fill effects

CURRENT EFFORT

A trade-off was done, considering the results of the previous section combined with the overall projected costs, to determine what type of system should be pursued. The results of the trade-off indicated that 35 GHz would be most suitable for the purposes of this effort. The following design will therefore consider only a 35-GHz system.

This portion of the planned two-year program is concerned primarily with the construction of a 35-GHz radiometer and its integration with a mobile tracking mount and the required data acquisition instrumentation. Growth potential is such that the passive system could be expanded into a low-power, frequency modulated continuous wave (FMCW) tracking radar or a high-power pulsed radar with only slight modifications. Areas requiring such changes to convert the radiometer have been taken into account in the design of the system and the procurement of hardware items.

RECEIVER DESIGN

The following listing is a summary of specifications for each of the most critical items in the receiver. A representative antenna pattern appears in Figure 7.

MIXER/LO/IF AMPLIFIER

Input RF center frequency	35 GHz
RF bandwidth	1 GHz
IF bandwidth	5-500 MHz
Noise figure	5.2 dB (measured) 5.5 dB (max)
RF/IF gain	25 dB (min)
RF voltage standing wave ratio (VSWR)	2.0:1 (max)
IF VSWR	2.0:1 (max)
LO electronic tuning	± 250 MHz (min)
LO mechanical tuning	± 50 MHz (min)
LO tuning voltage	+4 to - 24 V (typ)
Frequency stability	60 ppm/°C (max)
RF to LO isolation	20 dB (min)
IF compression (10 dBm IF output)	1 dB (max)

RECEIVER CON-SCAN ANTENNA AND FEED

RF center frequency	35 GHz
Dish diameter	3 ft (nom)
Gain	44 dB (min)
Beam width	0.7° (max) @ 3 dB points

Bandwidth	5% (min)
Side-lobe level	- 16 dB (max)
	- 15.6 to - 21.4 dB (measured)
Crossover point	3 dB
Nominal pattern shape	Sin x/x (main lobe)

The modular feed system allows selection of the following polarizations:

1. Circular (right hand)
2. Circular (left hand)
3. Horizontal linear
4. Vertical linear

Feed Specifications:

Center frequency	35 GHz
VSWR	1.35:1 (max)
Axial ratio	1.4:1 (max)
Isolation	25 dB (min)
Bandwidth	5% (min)
Attenuation	0.3 dB (max)

CASSEGRAIN TRANSMITTER ANTENNA

Center frequency	35 GHz
Dish diameter	2 ft (nom)
Gain	43 dB (min)
Beam width	1° (max) @ 3 dB points
Bandwidth	5% (min)
Side-lobe level	- 18 dB (max)
	- 18.0 to - 27.3 dB (measured)
Nominal pattern shape	Sin x/x (main lobe)
Aperture efficiency	50% (nom)

The modular feed system allows selection of the following polarizations:

1. Circular (right or left hand)
2. Horizontal linear
3. Vertical linear

Feed Specifications:

Center frequency	35 GHz
VSWR	1.35:1 (max)
Axial ratio	1.4:1 (max)
Isolation	25 dB (min)
Bandwidth	5% (min)

WAVEGUIDE SWITCH, ANTENNA FEED SELECTION

4-port, 2-channel	
Frequency	35 GHz
VSWR	1.05:1 (max)
Insertion loss	0.5 dB (max)
Average power capability	1 W (max)
Isolation	60 dB (min)

LATCHING FERRITE SWITCH, 3-PORT DICKE SWITCH

Center frequency	35 GHz
Bandwidth	± 500 MHz (min)
Isolation	20 dB (min)
Insertion loss	0.5 dB (max)
Switching time	1 μs (max) to 97% input power
Power capability	100 mW (max)
Drive voltage	TTL compatible
VSWR	1.3:1 (max)
Switching rate	dc to 15 kHz

NOISE TUBE REFERENCE

Center frequency	35 GHz
Excess noise ratio	15.4 dB ± 5 dB
VSWR (hot)	1.2:1 (max)
VSWR (cold)	1.3:1 (max)
Argon gas with Kr 85 additive	

TEMPERATURE CONTROLLED REFERENCE HOT LOAD

Center frequency	35 GHz
Load temperature	80°C to 90°C
Temperature stability	± 0.3°C (max)
VSWR	1.1:1 (max)

LIQUID NITROGEN REFERENCE COLD LOAD

Center frequency	35 GHz
VSWR	1.1:1 (max)
Flask capacity	2 qt of N_2 (refillable)
Load temperature	77.35°K (nom)

CURRENT CONTROLLED FERRITE ATTENUATOR

Center frequency	35 GHz
Bandwidth	± 500 MHz
Attenuator range	0 to 50 dB (max)
Insertion loss	1.6 dB (max)
VSWR	1.2:1 (max)
Control current	0 to 100 ma (max)
Average power	1 W (min)
Peak power	10 W (min)

WAVEGUIDE SWITCH, REFERENCE LOAD SELECTION

4-port, 3-channel	
Center frequency	35 GHz
Bandwidth	± 2% (min)
Insertion loss	0.3 dB (max)
VSWR	1.15:1 (max)
Isolation	40 dB (min)

These specifications provide the parameters for the design to follow.

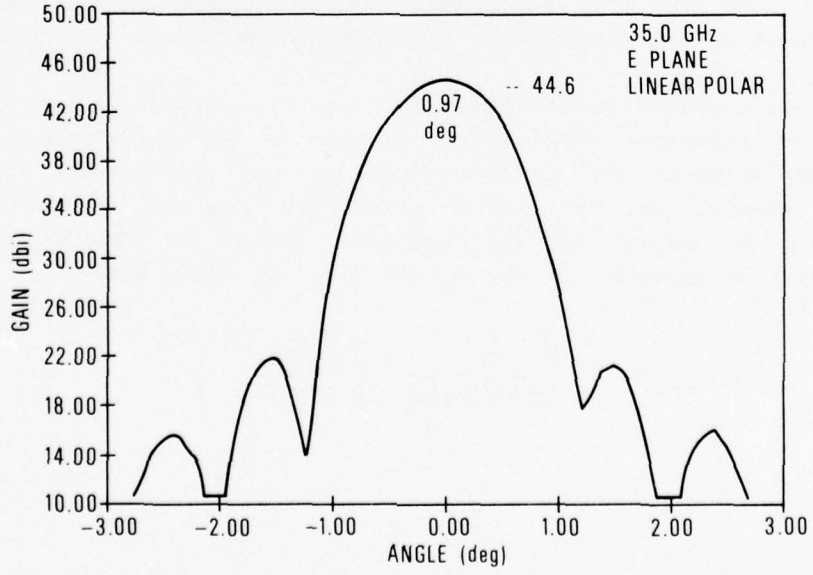

Figure 7. TRG Model A823-24C Antenna Pattern

The basic approach to the design was to use the best state-of-the-art devices available within the cost constraints dictated by the present level of funding. The impact of this constraint was felt mostly in the selection of the receiver/mixer. Originally, a 3-dB noise figure, 15-dB gain, uncooled paramp was selected. Assuming that a 7-dB noise figure mixer is used to provide a 3.3-dB overall amp/mixer noise figure, the cost was projected at approximately $45K. It was felt that a state-of-the-art low noise (5.5 dB) mixer alone could provide an acceptable noise figure for approximately 10 percent of this cost. Although this cost is much more realistic with respect to the funding level available, it would result in a 2-dB sacrifice in the receiver noise figure. To analyze the effect this difference in performance would have on system sensitivity, a receiver type first had to be specified.

Three receiver types are being considered for the IED system:

1. Superheterodyne

2. Correlation

3. Dicke

System performance of each receiver will be analyzed and evaluated as to its technical merits for use in a measurement quality radiometer. The two most critical parameters of the receiver are its overall system sensitivity and cost.

The superheterodyne receiver (Figure 8) is a total power receiver that is widely used in millimeter wave systems because of its good noise qualities and low cost. However, the superheterodyne has one problem – its sensitivity is critically dependent on the receiver predetection gain and its fluctuations. The sensitivity is defined as the minimum change in effective antenna temperature that is equivalent to the system noise or, from Kraus:[3]

$$\Delta T_{min} = T_{sys}\left(\frac{1}{\Delta f(Hf)\tau(Lf)} + \left(\frac{\Delta G(Hf)}{G(Hf)}\right)^2\right)^{1/2} \qquad (24)$$

where

ΔT_{min} = sensitivity
T_{sys} = system temperature
$\Delta f(Hf)$ = predetection bandwidth
$\tau(Lf)$ = postdetection integration time constant
$G(Hf)$ = predetection gain
$\Delta G(Hf)$ = predetection gain variation

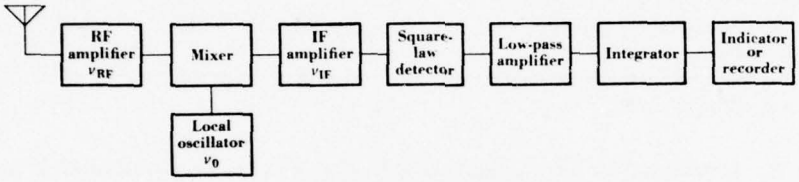

Figure 8. A Superheterodyne Radio-Telescope Receiver[3]

To determine the magnitude of this effect an example of a system is given with a 0.05 percent gain variation. Using Tables 7[3] and 8,[3] and for:

T_{sys} = 1113°K ≅ 6.8 dB system noise temperature + 15°K antenna temperature
$\Delta f(Hf)$ = 1 GHz
$\tau(Lf)$ = 0.135 sec, integrator
$G(Hf)$ = 75 dB
$\Delta G(Hf)/G(Hf)$ = 0.0005

and substituting into Equation 24 yields a ΔT_{min} of:

$$\Delta T_{min} = 0.095°K \quad \text{for:} \quad \Delta G = 0\% \tag{25}$$

$$\Delta T_{min} = 0.565°K \quad \text{for:} \quad \Delta G = 0.05\% \tag{26}$$

Table 7. Postdetection Equivalent Bandwidth $\Delta\nu_{LF}$ as Compared With Half-Power Bandwidth $\Delta\nu$ and Equivalent Integration Time t_{LF}[3]

Type of filter	$G_{LF}(\nu)$	$\Delta\nu_{LF}$	t_{LF}
Pure integrator, integrating time t_{LF}	$\frac{\sin^2(\frac{1}{2}\omega t_{LF})}{(\frac{1}{2}\omega t_{LF})^2}$	$\frac{1}{2t_{LF}}$	t_{LF}
Ideal low-pass filter	1	$\Delta\nu$	$1/2\Delta\nu$
n RC filters in independent cascade, time constant t_{RC}	$(1+\omega^2 t_{RC}^2)^{-n}$		
$n = 1$		$1.57\Delta\nu$	$2t_{RC}$
$n = 2$		$1.22\Delta\nu$	$4t_{RC}$
$n = \infty$ (Gaussian)		$1.06\Delta\nu$	$1/2.12\Delta\nu$
Second-order filter (ω_0 = undamped natural frequency of the filter; ζ = damping constant)	$\frac{\omega_0^4}{(\omega_0^2-\omega^2)^2+(2\zeta\omega\omega_0)^2}$	$\frac{\omega_0}{8\zeta}$	$\frac{4\zeta}{\omega_0}$

$\Delta\nu$ = 3-dB bandwidth

Table 8. Predetection Equivalent Bandwidth $\Delta\nu_{HF}$ as Compared With Half-Power Bandwidth $\Delta\nu$

Type of filter	$G(\nu)$	$\Delta\nu_{HF}/\Delta\nu$
n cascaded single-tuned stages	$\left[1+\left(\frac{\Delta\omega}{\pi\,\Delta\nu_s}\right)^2\right]^{-n}$	
$n = 1$		3.14
$n = 2$		1.96
$n = 3$		1.76
$n = 5$		1.62
$n = \infty$ (Gaussian)	$2^{-[\Delta\omega/(\pi\Delta\nu)]^2}$	1.50
m cascaded $2n$-pole Butterworth filters	$\left[1+\left(\frac{\Delta\omega}{\pi\,\Delta\nu_s}\right)^{2n}\right]^{-m}$	
$m = 1, n = 2$		1.48
$m = 1, n = 3$		1.26
$m = 1, n = \infty$		1.00
$m = 2, n = 2$		1.30

$\Delta\omega = \omega - \omega_0$, where ω_0 = angular center frequency
$\Delta\nu_s$ = 3-dB bandwidth of a single section
$\Delta\nu$ = 3-dB bandwidth of the amplifier

The sensitivity change resulting from a 0.05 percent gain variation is an order of magnitude larger than the 0 percent value. This result can be equated to an equivalent increase in T_{sys} by a factor of 10 or, equivalently, an increase in the system noise figure of approximately 10 dB. A more desirable receiver type should be sought since a measurements quality radiometer should be able to resolve down to a few tenths of a degree change in target temperature. The gain stability of the example would be very hard to achieve in practice; it is very expensive, and it does not produce the required sensitivity stability for the measurements program.

An attractive alternative is a correlation receiver. This receiver takes advantage of the fact that the gain variations of two separate receiver systems are not generally correlated in time. Only correlated signals produce a dc response in this type of receiver, and any uncorrelated noise input or gain variation will produce no correlated response. The receiver, as diagrammed in Figure 9, has a better sensitivity:[3]

$$\Delta T_{min} = \frac{1}{\sqrt{2}\cos\phi} T_{sys} \left(\frac{1}{\Delta f(Hf)\tau(Lf)} \right)^{1/2} \tag{27}$$

where

ϕ = relative phase of the two receiver channels

This, however, shows a slight sensitivity to small phase differences. A difference in phase of 10° would yield a change in sensitivity by a factor of only 1.015. The basic difficulty with this type of receiver is that its cost is essentially doubled by its requirement for two receiver channels, although its sensitivity is improved by a factor of $\sqrt{2}$ over the superheterodyne.

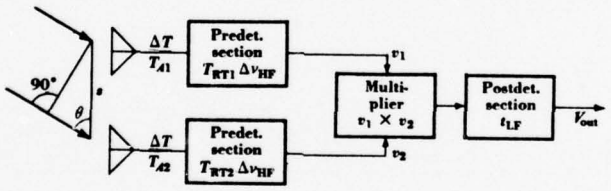

Figure 9. Interferometer With Correlation Receiver[3]

A third type of receiver, known as the Dicke receiver, takes advantage of the fact that gain fluctuations occur rather slowly so that the receiver can be rapidly switched between the antenna and a known reference source while the predetection gain stays essentially constant. A block diagram of this type of receiver is shown in Figure 10. By making the reference temperature equal to the antenna temperature, the receiver signal power becomes:[3]

$$P_s = K\Delta T\Delta f(Hf) \tag{28}$$

where

P_s = receiver signal power
K = Boltzman's constant
ΔT = signal temperature
$\Delta f(Hf)$ = predetection bandwidth

and is square-wave modulated at the switching frequency. The effect of predetection gain variation on sensitivity has been shown to be:[3]

$$\Delta T_G = (T_A - T_L) \frac{\Delta G(Hf)}{G(Hf)} \tag{29}$$

where

ΔT_G = change in sensitivity due to gain variations
T_A = antenna temperature
T_L = reference load temperature
$G(Hf)$ = predetection gain
$\Delta G(Hf)$ = predetection gain variation

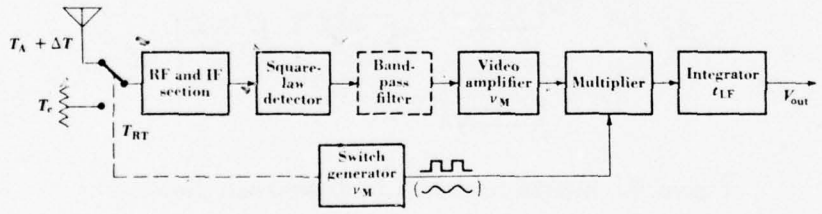

Figure 10. Switched or Dicke Receiver (Bandpass Filter Optional)[3]

By keeping $T_L \simeq T_A$, this change in sensitivity can be made very small and virtually independent of $\Delta G(Hf)$. The only major disadvantage of the Dicke receiver is its absolute sensitivity. This can be expressed as:[3]

$$\Delta T_{min} = 2\, T_{sys} \left(\frac{1}{\Delta f(Hf)\tau(Lf)} \right)^{1/2} \tag{30}$$

assuming a 50 percent duty factor for the Dicke switch. This is one-half the sensitivity of the superheterodyne, equivalent to an increase in noise figure of 3 dB. Comparing this with the sensitivity of the example system in Equation 24 would yield:

$$\Delta T_{min} \simeq 0.2°K \tag{31}$$

This reduction in sensitivity, while undesirable, is less degrading than the superheterodyne sensitivity variations. In addition, the cost of this type of receiver is more attractive than that of the correlation receiver because it uses only one receiver channel. For these reasons, the Dicke is seen as a good compromise between the superheterodyne and the correlation receiver types.

Several other factors also dictate the sensitivity that the radiometer, as a system, will have. The waveguide losses between the receiver and the antenna are the primary causes, other than the receiver, of sensitivity loss because these losses increase the overall system noise temperature, or noise figure, which is shown as a direct reduction of the sensitivity. Including the effects of the antenna temperature, the overall system noise temperature is:[12]

$$T_{sys} = T_A + L\,T_R + T_o(L - 1) \tag{32}$$

where

T_{sys} = overall system temperature
T_A = antenna temperature
T_R = equivalent receiver noise temperature
T_o = attenuator temperature (ambient)
L = attenuator loss factor

This loss, L, is defined as the reciprocal of the attenuator gain; therefore, L is always greater than unity. Also, the loss factor, expressed in dB, adds directly to the system noise figure, expressed in dB.

With this knowledge of how system losses, receiver type, and noise figure are related and interact, a good estimate of system sensitivity can be made, given data on the components used in the system front end. However, because of the nature of the measurements program and receiver type, many components not normally associated with other receivers will be used in the front end (Figure 11). These components and their effects are discussed below.

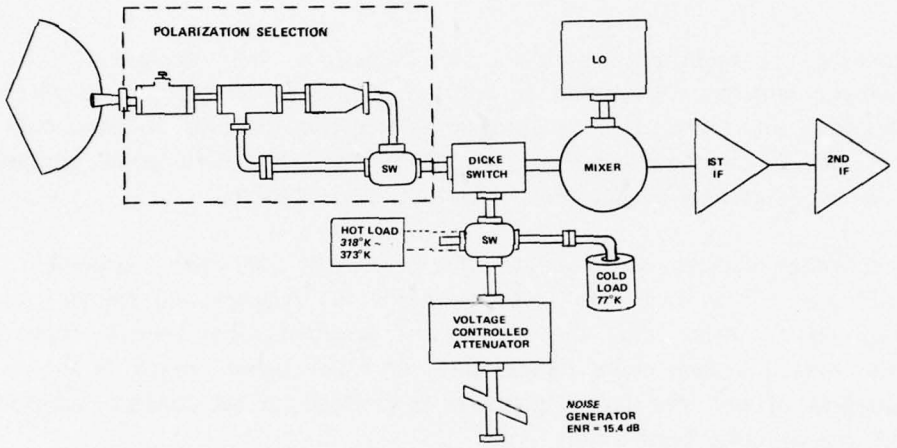

Figure 11. 35-GHz Passive Receiver Front End and IF

The data sought in this program is dependent, among other parameters, on polarization. For complete and meaningful measurements, therefore, some kind of polarization agility must be designed into the system. This requirement has been met by specifying in the antenna and feed system contract that manual selection of polarization be included. As the antenna and feed are configured (Figure 11), there is 0.3 dB (max) loss in the feed assembly and an additional 1.0 dB (max) total loss in the polarization and Dicke switches. Using the 5.5 dB mixer/IF amplifier combination, as specified earlier, would yield an overall receiver noise figure of 6.8 dB. This figure converts to a noise temperature of approximately 1098°K. If the original paramp were used instead, the overall noise figure would be approximately 4.8 dB, or 586°K. The antenna temperature, however, has still not been accounted for. In most cases (as in this case), the antenna temperature is approximately 15°K. Adding this figure to the results above give 1113°K for the low noise mixer and 600°K for the paramp. Using Equation 30, the sensitivity for a Dicke receiver is:

$$\Delta T_{min} = 2\, T_{sys} \left(\frac{1}{\Delta f(Hf)\tau(Lf)} \right)^{1/2} \tag{33}$$

$$= 2(1113) \left(\frac{1}{10^9 \times 0.135} \right)^{1/2} \tag{34}$$

$$= 0.19°K \text{ for low noise mixer} \tag{35}$$

$$\Delta T_{min} = 2(600) \left(\frac{1}{10^9 \times 0.135} \right)^{1/2} \tag{36}$$

$$= 0.10°K \text{ for paramp} \tag{37}$$

for

$\Delta f(Hf)$ = 1-GHz receiver bandwidth
$\tau(Lf)$ = 0.135-sec integration time from following section

The use of the low noise paramp provides only an additional 0.1°K increase in sensitivity; this is not a significant improvement for the additional cost of the paramp.

Actual measurements on the low-noise mixer and feed system indicate a noise figure of 6.8 dB (max) which is identical to the figure used in the preceding analysis. This sensitivity, therefore, is that which is expected in the receiver.

The end result of the receiver design is shown in Figure 12. This figure shows the completed receiver prior to the delivery of the antennas.

SIGNAL PROCESSING

Use of a Dicke switched receiver results in the requirement for a synchronous demodulator after the video detector and comb filter (Figure 13). This is characteristic of all Dicke receivers because the dc output of the receiver is modulated at the Dicke switch rate. The synchronous demodulator effectively reverses the signal polarity in synchronism with the Dicke switch to produce the unsmoothed dc level shown in Figure 14. This is then integrated to produce the radiometer output, also shown in Figure 14. The smoothing will involve filtering, or

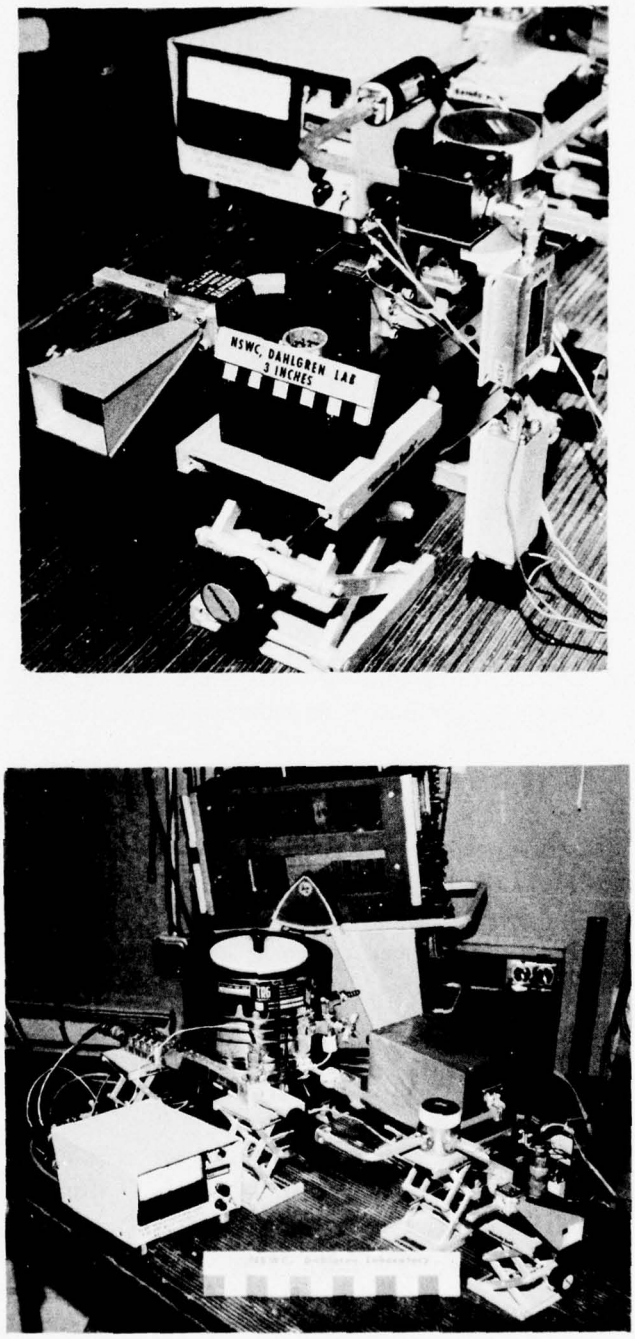

Figure 12. Front and Side Views of 35-GHz Passive Radiometer Receiver

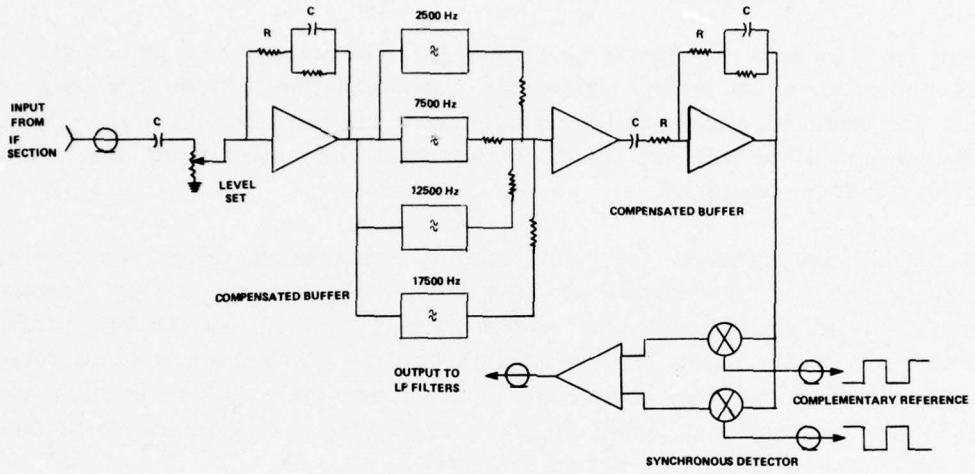

Figure 13. Filter and Synchronous Detector

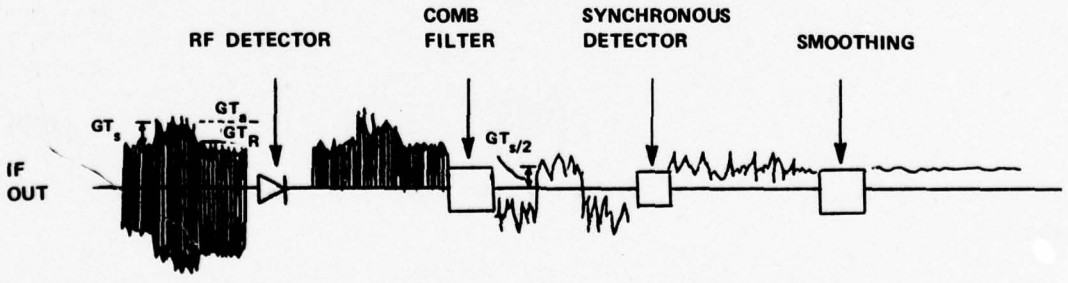

Figure 14. Synchronous Detection Waveform in the LF Section of a Radiometer

integrating, to maximize the receiver sensitivity for a given type of measurement. The longest integration time will be used while making background profile measurements; the shortest integration time will be used for passive tracking and will be determined by the con-scan rate and angular resolution required.

There are a number of variable parameters that are not precisely known at this point in the program. A certain amount of experimentation will be necessary to determine the best and most useful integration time constants for the various types of measurements. These will be chosen to minimize the measurement time while maintaining maximum sensitivity.

A rough approximation of the required integration time for profile measurements can be determined by considering the tracking mount dynamic characteristics in conjunction with the amount of data required. An elevation profile at 2° increments over a sector 180° in azimuth by 100° in elevation is to be taken in 7 to 8 min. This can be accomplished by measuring every 10° in azimuth and allowing 0.5 sec for each data point in elevation, yielding a total measurement time of 7.75 min, which is within the desired time frame.

Taking the measurements every 2° vertically essentially fixes the maximum integration time in the processor. Assuming an ideal mount response with a step acceleration and deceleration applied, then the minimum time to traverse 2° is:

$$\theta = 2\left(1/2\, a \left(\frac{T}{2}\right)^2\right) \tag{38}$$

or

$$T = \left(\frac{(4\theta)}{a}\right)^{1/2} \tag{39}$$

where

T = time to move 2° and stop
θ = angle traversed = 2°
a = angular acceleration of mount = 60°/sec^2

This will yield a travel time of:

$$T = \left(\frac{4(2)}{60}\right)^{1/2} = 0.365 \text{ sec} \tag{40}$$

Subtracting this time from the total data point acquisition time of 0.5 sec will yield 0.135 sec for actual measurement time. This is the same integration time used in the Receiver Design section for the calculation of sensitivity This number should be reasonable for adequate sensitivity and will be maintained as the minimum integration time desirable for the Dicke receiver in modes other than tracking.

Another, and in most cases perhaps more desirable, method of scanning the mount over the desired field of view involves breaking the vertical scan into separate regions where different vertical resolutions can be used. Similar studies[13] have shown that the temperature profiles are rather constant from zenith down to approximately 60° from zenith, requiring lowest resolution at near zenith angles and highest resolution at the lower angles. By dividing the scan into two 30° segments and one 40° segment, approximately the same overall scan time and temperature sensitivity can be realized while increasing the angular resolution for the low angles. This is accomplished by taking measurements at 4° intervals from zenith (90°) down to 60°, then at 3° intervals down to 30°, and finally at 1° intervals down to -10° elevation. Using the same type of analysis as given earlier, a total vertical scan time of 26.7 sec will be achieved as compared with the original 25 sec. The integrating time of 0.135 sec will also be maintained in this type of scan. The total scan time will be 8.3 min as opposed to 7.75 min for the previous method.

Each type of scan can be used for profiling, depending on the weather conditions. Because the scanning mechanism will be microprocessor controlled, only a change in software will be necessary. The measurement time can also be changed, within limits, by modifying these schemes and accepting different angular resolutions.

To realistically correlate this type of data with environmental conditions, it is necessary to record at these high data rates. Manual control of the mount will not provide the capability of executing this task in a timely manner, and the usefulness of the data will be degraded.

The second type of measurement envisioned is passive imaging (mainly of ship targets), the most critical element of which is the time involved to make the measurements. Since most of the targets likely to be encountered will be ship targets of opportunity entering or leaving the harbor, the ship motion relative to the

background will cause the target/background temperature contrast to change with time rather rapidly. The target aspect could also change rapidly and cause further problems. Therefore, the imaging time must be very short with respect to target motion or some kind of compensatory imaging routine must be devised. The method envisioned at this point is to scan the target vertically along a fixed azimuth position and allow the target to pass at its own speed. This will allow the use of a constant background to act as a reference which will hopefully allow operation of the receiver as a total power receiver, similar to the tracking case, and thus improve its sensitivity by a factor of two. The reference point will be the starting point of each vertical scan. Also, by determining the angular rate of the target just prior to its entering the test region, a compensating azimuth rate can be included in the scan to make the measurement slice vertical with respect to the target structure. This will eliminate any azimuth smearing of the temperature profile.

This scan will be a constant angular velocity scan to reduce the overall scan time and complexity. The velocity chosen will be dependent on a number of parameters including, but not limited to, target velocity, target range, target type, and required resolution. The actual mount control will again be microprocessor controlled to maximize scan efficiency. The specific scan controls and time constants will vary over a large range of possibilities and cannot be analyzed completely here. Much will be dependent on the individual test conditions at any given time. However, to maintain the 0.2°K resolution as for the profile measurents, the integration time will have to be at least 31 ms for the total power receiver. This will allow approximately 32 elements of resolution in 1 sec, a reasonable vertical scan time for almost any test condition expected.

Passive radiometric tracking will also be a desired operating mode. The integration time will be determined, primarily, by the scan rate. With a high con-scan rate, the receiver gain should not drift significantly during the period of one or two scans. Therefore, the radiometer can resolve the temperature differences occurring within this scan period and the con-scan will, in effect, provide the Dicke action. The major disadvantage is the very short integration time. For a 10° angle resolution and a con-scan rate of 125 Hz, the maximum integration time will be approximately 0.22 ms. This is three orders of magnitude smaller than that for the background measurements. This integration time will yield a sensitivity of 2.4°K. During the integration period, the receiver is acting as a total power receiver and is not Dicke in nature; therefore, this sensitivity figure is a factor of two better than that calculated using the Dicke sensitivity equation. Reducing the scan rate to 70 Hz will increase the maximum sensitivity by approximately 0.6°K (making Δt smaller). However, it is not clear at this time what the time characteristics of the

receiver gain fluctuations will be, so that some uncertainty exists as to the minimum scan rate that will provide reliable error signals. This lower scan rate will, however, result in the possibility of using the Dicke switch within each scan cycle, if necessary, to compensate for sensitivity variations. Using the projected 2.5-kHz Dicke switch rate will yield an integration time of 0.4 ms; this translates into a sensitivity of 3.5°K. The slower scan rates will be used to evaluate the tracking system and to determine whether higher scan rates will be needed.

The predicted detection ranges will be a function of many parameters, but perhaps the most critical will be the target passive "cross section." These cross sections and detection ranges will be the subject of Volume II, Confidential TR-3749, entitled ***Surface Navy Applications of Millimeter Wave Sensors, Predicted Detection Range Performance of the NSWC IED Passive Millimeter Wave Sensor.***

INSTRUMENTATION

All the measurements discussed so far will use a microprocessor controlled data acquisition system. The radiometer output signal will be sampled with high-speed, sample/hold modules, and the data will be stored on magnetic tape for off-line data reduction. The only real-time data reduction will occur during tracking tests and for any mount positioning functions that are required in the measurements. The radiometer output, in conjunction with mount error signals, will be recorded on digital magnetic tape in all cases for later analysis and comparison with the instrumentation and high resolution camera video. A DBA optical tracking system will be used to reduce the camera data, recorded on video tape, into a digital format.

Present intentions are to monitor all the hardware parameters pertinent to the tests conducted (Figure 15). These include LO tuning voltage, reference load attenuator voltage, video amplifier AGC voltage, waveguide switch positions, radiometer output, polarization, antenna boresight error signals, mount position, and mount velocity. These signals will all be multiplexed at the mount and digitized, if necessary, for transmission to the instrumentation suite (Figure 16). Any real-time processing required will then be performed along with the long term data storage processing. Also shown in the figure are a variety of system monitoring signals that will be used to provide system operating data and malfunction indications.

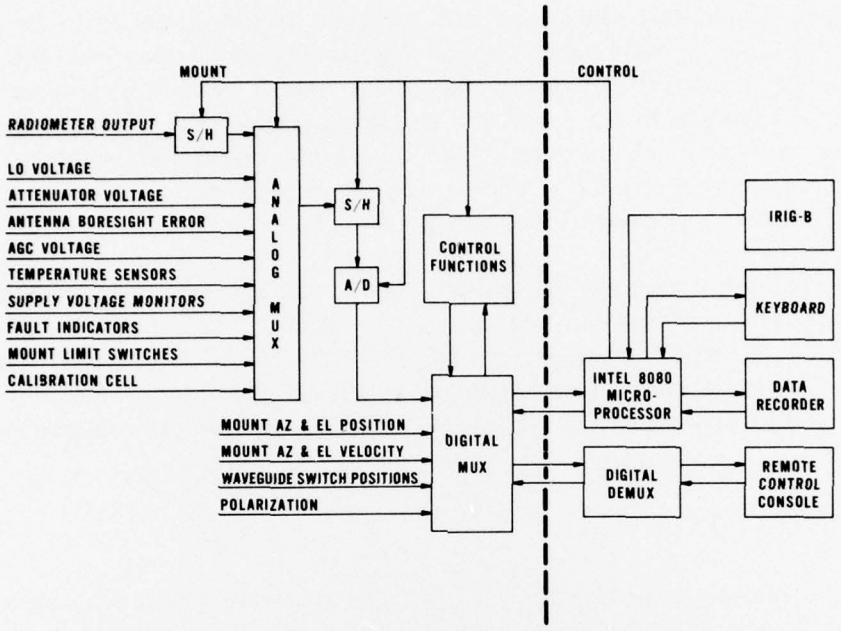

Figure 15. System Instrumentation

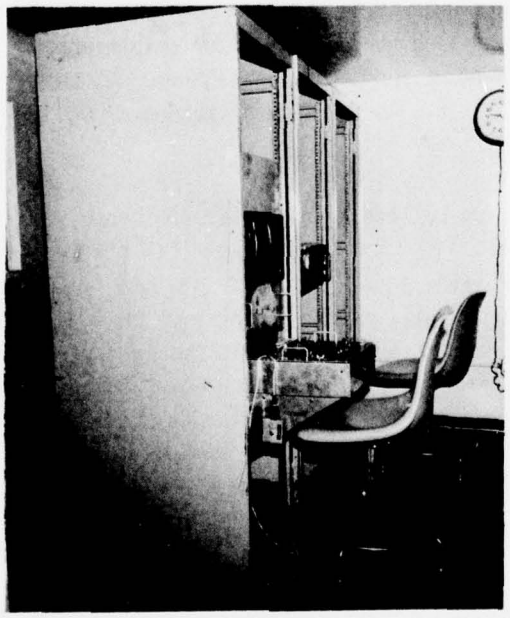

Figure 16. Proposed Instrumentation Suite

The instrumentation, as conceived, will provide a maximum degree of flexibility while providing the greatest depth in data acquisition capability. This is mainly due to the high data transfer rate of the Model 8107 Kennedy Recorder. The recorder will take data in 19K-bit chunks at 1 μsec/character (7 bit ASCII) and store the data in approximately 20 μsec. It also has a latching buffer that can be loaded while the recorder is dumping from a second buffer. As mentioned earlier, all the data acquisition and timing will be controlled by the microprocessor for maximum efficiency.

OPTICAL TRACKING MOUNT

Originally, the Geo Space Corporation mount (Figure 17), was used at the Naval Ordnance Missile Test Facilities, White Sands, New Mexico as an optical tracking mount. Locally, it was acquired by NSWC/DL as surplus equipment. Time was spent in refurbishing the mount because of its degenerated condition. The mount was repaired and tested and should now meet the original specifications outlined in Table 9. Figures 18 and 19 show how the receiver will interface to the mount. Figure 19 shows the receiver mounted behind the 2-ft dish, the configuration to be used in most of the measurement and imaging tests.

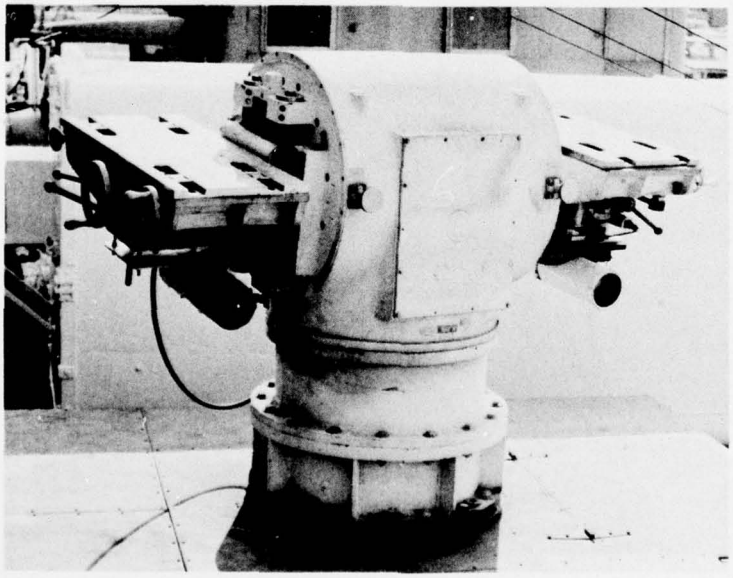

Figure 17. Geo Space Optical Tracking Mount

Table 9. Mobile Optical Tracking System

Pointing Errors		
	Positioning	
	Static	10 μrad
	Dynamic	3 μrad/mr/sec
	Velocity	30°/sec
	Acceleration	60°/sec²
Displacement		
	Azimuth	±170°
	Elevation	-10° to +90°
Data		
	13-bit digital angle resolution (768 μrad)	

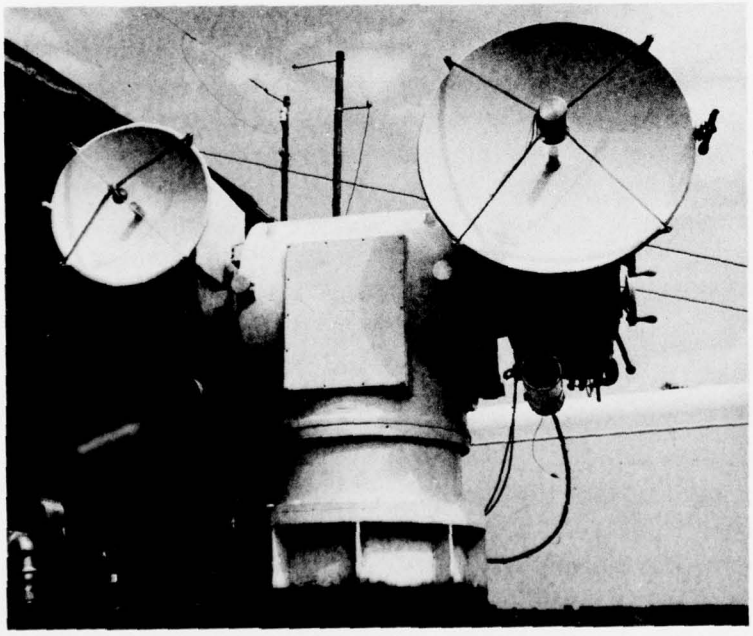

Figure 18. System Mount Configuration

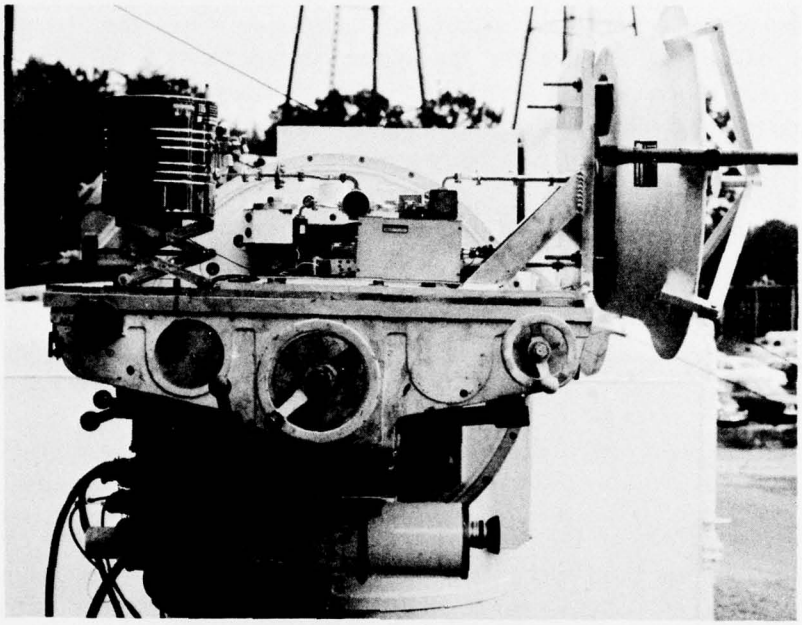

Figure 19. Final Receiver Configuration

PLANNED TEST PHASE

Initial testing of the radiometer will be performed at Dahlgren as part of the hardware processing design phase. System parameters and performance will be established and hardware configurations will be firmed. It is expected that initial testing will be completed by the end of December with some initial background measurement data taken at Dahlgren.

The initial phase will be followed by approximately 10 weeks of intensive measurements at Dahlgren. This phase will consist mainly of background and sky-sea-land interface measurements under a variety of combinations of weather, polarization, and, in some cases, processing conditions. Some imaging and tracking of range boats and ship targets-of-opportunity will also be conducted to provide baseline performance in this mode. This baseline will be used to develop the processing software and hardware prior to the final phase of the measurements program.

Finally, the system will be moved to Norfolk to do ship measurements on surface combatants and possibly submarines. Background measurements will also be performed to establish a baseline for the system in the Norfolk environment. These measurements will be conducted entirely with targets-of-opportunity; there will be no scheduled targets other than calibration targets. Surface and aircraft tracking, with targets-of-opportunity only, may also be investigated at Norfolk.

All system testing is scheduled for completion by the end of June. This will allow approximately 3 months to conclude the data reduction and formatting for the final report.

CONCLUSIONS

The first-year effort of the two-year millimeter wave IED program, as defined in the Introduction, has been successfully completed. It was shown that the goals of this effort complement other efforts, both in-house and at other activities, by making available additional measurements for the NSWC millimeter wave data base and by providing in-house expertise in millimeter wave hardware.

Although a complete analysis was not given, the operating frequency of 35 GHz was selected as the most desirable frequency on the basis of overall system sensitivity, and resolution requirements as well as component availability and costs. The receiver has been designed and built, and the measured system noise figure is a maximum of 6.8 dB. This will yield a receiver sensitivity of approximately 0.2°K for the background measurements and approximately 3.5°K in the tracking mode. These figures are considered adequate for the program and should produce the desired results. The system noise figure was very close to the design goal of 7.2 dB (max) which indicates the validity and accuracy of the design methods used and of the manufacturer's specifications. However, component technology has advanced somewhat since the design was firmed, and slightly improved results should be expected in future designs.

It was found that all the system controls and data acquisition requirements could not be efficiently controlled manually; therefore, it was decided to use a microprocessor for control functions and data acquisition to allow maximum processing efficiency and flexibility. This, in turn, will allow a more flexible overall measurements program with more consistent and reliable results and will use to greater advantage the data reduction capabilities of the CDC 6700 computer.

Fiscal year 1978 will be far more productive in terms of measurements, and the experience and data gained will be well worth the effort and costs.

REFERENCES

1. R. A. Holden and D. F. Hudson, ***Relative Accuracy and Operational Effectiveness of Laser Guided Weapons for USMC Applications***, NSWC/DL Technical Report TR-3376, September 1975.

2. R. Stump, ***Microwave Radiometric Terminally Aimed Bomb Study (MICRAD)***, NSWC/DL Technical Report (in preparation).

3. J. D. Kraus, Ph.D., ***Radio Astronomy***, McGraw-Hill Book Company, 1966.

4. ***Radiometric Range Handbook***, Singer-General Precision, Inc., Kearfott Division, ETO-882-32.

5. V. W. Richard, ***Millimeter Wave Radar Applications to Weapons Systems***, Ballistic Research Laboratories Memorandum Report 2631, June 1976.

6. V. W. Richard and J. E. Kammerer, ***Rain Backscatter Measurements and Theory at Millimeter Wavelengths***, Ballistic Research Laboratories Memorandum Report 1838, October 1975.

7. E. S. Rosenblum, ***Atmospheric Absorption of 10 to 400 KMcps Radiation***, Microwave Journal, March 1961, pp. 91-96.

8. ***TRG Millimeter Microwave Products and Capabilities***, TRG Division, ALPHA Industries, Inc., 1976.

9. N. C. Currie, F. B. Dyer, and R. H. Hayes, ***Analysis of a Radar Rain Return at Frequencies of 9.375, 35, 70 and 95 GHz***, Georgia Institute of Technology, Atlanta Engineering Experiment Station, February 1975.

10. C. A. Samson, L. G. Hause, and A. P. Barsis, ***Precipitation Attenuation Effects on Wideband Communication Links Above 10 GHz***, 1974 Millimeter Waves Techniques Conference, Naval Electronics Laboratory Center, 26-28 March 1974.

11. K. L. Koester and Dr. L. H. Kosowsky, ***Attenuation of Millimeter Waves in Fog***, Fourteenth Radar Meteorology Conference, 17-20 November 1970.

12. G. Evans and C. W. McLeish, ***RF Radiometer Handbook***, Artech, 1977.

13. R. S. Roeder, et. al., ***Millimeter Wave Semiactive Guidance System Concept Investigation***, SJ 242-8457-5, November 1976.

DISTRIBUTION

Naval Air Systems Command
Washington, DC 20360
ATTN: J. Willis (310B)
V. T. Tarulis (360E)
B. Glatt (03P24)
J. Malloy (03P)

Naval Weapons Center
China Lake, CA 93555
ATTN: P. Homer (390)
A. Shlanta (317)
R. P. Moore (3542)
J. Battles (3962)
W. Freitag (3981)
F. Alpers (35031)
W. Katzenstein (3542)
Technical Library

Picatinny Arsenal
Dover, NJ 07801
ATTN: Theodore Malgeri (SARPA-AD-D-W)

Army Missile Command
Redstone Arsenal, AL 35809
ATTN: A. H. Green (AMSMI-RER)
(DRSMI-RNX)

Naval Sea Systems Command
Washington, DC 20360
ATTN: CAPT Organ (NSEA-034)
T. Tasaka (NSEA-03415)
CDR E. L. Christensen (NSEA-06G1)
R. Hill (06522)
CDR Nelson (06532)
CDR Dunn (PMS-404-40)
J. Whalen (06543)

Naval Air Development Center
Johnsville, PA 18974
ATTN: M. Foral (2042)
Technical Library

Naval Research Laboratory
Washington, DC 20375
ATTN: Dr. Carmen Vittoria (7110)
Dr. B. Yaplee (7110)
Dr. B. Spielman (7110)

Air Force Armament Technology Laboratory
Eglin AFB, FL 32542
ATTN: C. Brown (DLMT)

Pacific Missile Test Center
Port Hueneme, CA 93041
ATTN: R. J. Schlapia (1231)

Ballistic Research Laboratory
Aberdeen Proving Ground, MD 21005
ATTN: K. Richer (DRXBR-CA)

Night Vision Laboratory
Fort Belvoir, VA 22060
ATTN: W. Ealy

Director of Defense Research and Engineering Technology
Washington, DC 20301
ATTN: Dr. D. Charvonia (3E114)

Office of Naval Research
800 North Quincy Street
Arlington, VA 22200
ATTN: CDR McCullough (ONR-212)
T. J. Horwath (ONR-220)
CDR D. C. Hanson (ONR-221)
(ONR-480)

Defense Advanced Research Projects Agency
1400 Wilson Boulevard
Arlington, VA 22209
ATTN: Dr. J. Tegnelia (TTO)
Dr. D. Walsh (STO)

Naval Material Command
Washington, DC 20360
ATTN: C. Lyons (08T2211)
CDR J. D. Tadlock (08T224)

Commanding General
Marine Corps Development and Education Command
Quantico, VA 22134
ATTN: Technical Library

Naval Oceans System Center
San Diego, CA 92152
ATTN: R. T. Kihm
R. Straight (7410)
Technical Library

MIRADCOM
Redstone Arsenal, AL 35809
ATTN: S. L. Johnston (DDPMI-CE)

Harry Diamond Laboratories
Adelphi, MD 20783
ATTN: Dr. S. Kulpa

U. S. Army Electronics Command
Fort Monmouth, NJ 07703
ATTN: Dr. H. Jacobs (AMSEL-TL-IJ)

Naval Electronics Systems Command
Washington, DC 20360
ATTN: R. Brooke (PME107-142)
Nate Butler (03)

Chief of Naval Operations
Department of the Navy
Washington, DC 20350
ATTN: LCDR W. L. Putnam (961D21)
CDR L. E. Krekel (961D3)
LCDR J. C. Hodell (955E)
CDR L. E. Pellock (982F3)
J. L. Kaminski (3511)

Defense Documentation Center
Cameron Station
Alexandria, VA 22314 (12)

Defense Printing Service
Washington Navy Yard
Washington, DC 20374

Library of Congress
Washington, DC 20540
ATTN: Gift and Exchange Division (4)

Local:

CA
CA-21
CC-01 (LCOL Bruner)
CC-06 (K. Cox)
CD-2 (D. B. Colby)
CD-02 (C. P. Hontgas)
CE
CF
CF-10
CF-14
CF-14 (Holden)
CF-14 (Harrop) (20)
CF-56 (V. G. Pugieilli)
CG
CG-20 (D. W. Culbertson)
CK
CK-61 (C. T. Shelton)
CK-74 (H. Thombs)
CN
CN-50 (K. C. Heppfer)
CN-80 (R. N. Cain)
CR
CT
CT-54 (L. L. Pater)
CU
DX-21 (2)
DX-222 (6)
DX-40
DX-43 (Elliott)
DX-43 (Green)